A THREE-DIMENSIONAL BIOMECHANICAL MODEL FOR PREDICTION OF GARMENT PRESSURE IN PRESSURE THERAPY FOR BURN PATIENTS

by

Lihuan ZHAO*, Jie YU, Siyu ZHANG, and Cuiyu LI

School of Textile Science and Engineering, Tiangong University, Tianjin, China

Original scientific paper
https://doi.org/10.2298/TSCI2004357Z

Compression garments produce a pressure to suppress and flatten hypertrophic scars caused by serious burns, and its value plays a critical role in the treatment. In this study, a 3-D biomechanical mathematical model is established to study numerically the pressure distribution over the arm given by a compression sleeve. The actual geometry of a female arm is used in our study, which is obtained from a 3-D reconstruction of computer X-ray tomography images. The arm model consists of bones and soft tissues, and the sleeve is described by an orthotropic shell model. The finite element method is adopted to predict the pressure distribution, which is then experimentally verified in a good agreement, providing a good understanding of the mechanism of pressure action on hypertrophic scars, and enhancing the medical function of a compression garment. The present method offers also a new approach to optimal design of compression garments with real constraints.

Key words: *computer X-ray tomography medical image, numerical simulation, pressure distribution, compression sleeves, hypertrophic scars*

Introduction

It has been reported that 91% of serious burns can lead to a serious complication called hypertrophic scarring [1]. Pressure therapy, which is simple, effective, inexpensive and non-invasive, is one of the most effective methods for suppressing and flattening hypertrophic scars [2].

The treatment principle of pressure therapy is that compression garments can produce pressure (namely, garment pressure) on human bodies. According to repeated clinical trials and studies, it has been reported that garment pressure from 20 mmHg to 25 mmHg sees the best therapeutic effect [3]. Therefore, to satisfy the precautionary and therapeutic effectiveness of hypertrophic scars, proper measurements and evaluations of the magnitudes and distributions of the applied skin pressures are very important.

To date, two main approaches have been widely undertaken to measure or evaluate garment pressure. The most popular method is direct testing based on pressure sensors. Many different types of pressure sensors, including hydrostatic pressure sensors [4], pneumatic pressure sensors [5] and electric pressure transducers [6], were used to determine the pressure given by a compression garment to the human body. However, in clinical practice, there is an

* Corresponding author, e-mail: zhaolihuan@tiangong.edu.cn

absence of actual measurements for garment-skin interface pressure to objectively monitor the efficiency of the pressure garment over time. Indirect estimations of pressure performances can be made by testing the physical properties of compression garment materials [7] or calculating garment pressure according to fabric tensile properties based on Laplace's equation [8]. These methods can help quantify and understand the garment pressure applied by the compression garments. However, some limitations still exist. At present, there are no testing devices that are able to test skin pressure over the entire surface of the body. Pressure sensors for use between the surface of the body and the compression garment with different dimensions and sensitivities have been introduced, which allow changes in the cross-sectional radius and subsequent changes in fabric tension over the sensor. However, these testing modes cannot exactly replicate and visualize the changing pressure profiles during wear.

Many scholars have studied the aforementioned problems and built models for compression garments that can apply garment pressure on the human body, the magnitudes and distribution of garment pressure of the whole compressed portion can be numerically simulated by the finite element method (FEM) before tailoring. Wong *et al.* [9] investigated numerically the distribution of garment pressure by tight-fitting sportswear. Luo *et al.* [10] presented a computable model to solve the problem of pressure distribution on the human body from tight underwear. Tarrier *et al.* [11] assembled 2-D fabric pieces into a 3-D garment in a process akin to sewing and gave a numerical approach to distributions of material strain and pressure on the body. Dan *et al.* [12] simulated displacement and pressure distribution on the human leg caused by men's socks by using the FEM to look for a functional relationship between pressure and displacement. Yu *et al.* [13] developed a biomechanical model for simulating the pressure magnitudes and distribution over the hand dorsum from a pressure glove using the FEM. Commercial human bodies or non-contact laser scanning data were used for constructing the models of the bodies in the aforementioned research. The models could not reflect the internal structures of the human bodies, which resulted in large performance differences with real human bodies, which contain soft tissues and bones. Human medical images obtained by computer X-ray tomography (CT) or magnetic resonance imaging technology [14] contain data on the internal structures of human bodies and can be used for constructing models consisting of skin, soft tissues, bones, *etc.*, which are closer to actual human characteristics. Therefore, the numerical simulations based on these models are more accurate.

As one of the most commonly burned parts of the human body, the arm was selected as the research object. A 3-D biomechanical model was developed to numerically simulate garment pressure exerted by a compression sleeve and based on the FE analysis in conjunction with objective pressure testing. Based on the simulation model, the pressure distribution on the arm can be visualized. The outcome of the pressure distribution can also offer a useful reference for adjusting, and thus enhancing, the quality and effectiveness of the treatment.

Methods – building the finite element model

A commercial FEM software, ABAQUS/CAE 2016, was used to carry out the simulation of the interaction between arm and sleeve. The interface pressure simulation model mainly consisted of two materials: an arm and a sleeve fabric. First, the geometry of the arm model was obtained from a 3-D reconstruction of CT coronal images from the right arm of a healthy Chinese female subject (age 50 years old, height 163 cm, weight 59.10 kg, body mass index 22.24 kg/m^2), since this was a trial test, no burn victims was recruited. Second, a 3-D geometric model of the sleeve was created. Third, the appropriate element type and material properties were defined. After meshing, the numerical processing of sleeve wear on an arm

was carried out to obtain the numerical solution. The pressure magnitudes and distribution over the arm could thus be simulated. Finally, the results were post-processed and validated.

Geometric model of arm and sleeve

Construction of the arm model

To study the pressure distribution on the arm, it is essential to develop a 3-D arm geometric model. To attain the anatomic structures of arm cross-sections, multiple CT images were taken with intervals of 1 mm in the neutral unloaded position. The MIMICS 15.0 was employed for filter processing, image segmentation, 3-D reconstruction of the skeleton and soft tissue, *etc.* Figures 1(a) and 1(d) show the skeleton and soft tissue models of the arm after 3-D reconstruction, respectively. Then, skeletal and soft tissue models of the human arm were imported to 3-Matic software for pre-treatment of finite element analysis. The surface was smoothed and reduced by 3-Matic, and the optimized processing was carried out. The processed images are shown in figs. 1(b) and 1(e). Finally, the mesh was divided to generate a C3-D4 type finite element linear tetrahedral mesh; as shown in figs. 1(c) and 1(f), the skeletal model consisted of 12494 elements with a minimum mesh size of 0.07 mm, while the soft tissue model consisted of 53638 elements with a minimum mesh size of 3.41 mm.

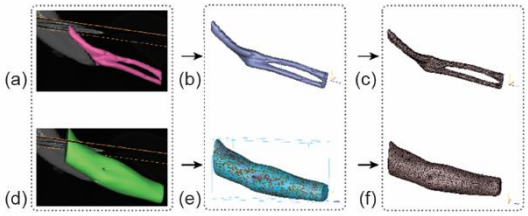

Figure 1. (a) The skeletal model, (b) optimized skeletal model, (c) the skeletal model after generating the body mesh, (d) the soft tissue model, (e) optimized soft tissue model, and (f) the tissue model after generating the body mesh

Development of sleeve model

A compression sleeve was used as the geometric prototype for simulating the digital sleeve model. According to the arm shape of the Chinese female subject previously described, a compression sleeve was made. The cylindrical sleeve was divided into 12 sections, 5 centimetres apart, fig. 2(a), the circumference of the cross-section of each section was calculated by the method of Maklewska *et al.* [8], and 24 mmHg pressure was set. Then, the 3-D digital compression sleeve model was constructed using the FE Package ABAQUS/CAE. Since the skeleton and soft tissue models of the arm were meshed in the pre-treatment, only the compression sleeve model needed to be meshed, the sleeve model after mesh generation is shown in fig. 2(b). The mesh element used for the sleeve fabric model was a linear quadrilateral shell element (S4R). There were 7743 elements in the sleeve fabric model, with a minimum mesh size of 2.47 mm.

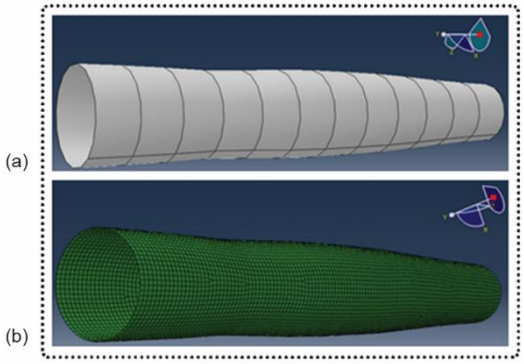

Figure 2. (a) The 3-D digital sleeve model with twelve sections and (b) the mesh generation of sleeve model in ABAQUS

Defining material properties

In this study, the simulation model has two material models: the arm and sleeve. The skeleton and the soft tissue were taken as flexible and compressible and assumed to have deformations during wear. They were defined as solid, homogeneous, isotropic, and linearly elastic biomaterials. The Young's modulus, Poisson's ratio, and mass density of soft tissues were taken as 0.5 MPa, 0.48, and $1.03e^{-9}$ tonne per mm^3, respectively. In addition, the Young's modulus, Poisson's ratio, and mass density of skeleton were taken as 7300 MPa, 0.30, and $1.85e^{6}$ tonne per mm^3, respectively.

The material properties of the compression sleeve were defined as orthotropic and linearly elastic. The parameters needed in the numerical analysis are listed in tab. 1, where E_1 and E_2 represent the Young's modulus in the course and wale directions, respectively. The G_{12} and υ_1 denote the shear modulus and Poisson ratio, and T is the fabric thickness.

Table 1. Material properties of the compression sleeve

W [tonne per mm^3]	E_1 [Nmm^{-2}]	E_2 [Nmm^{-2}]	G_{12} [$NNmm^{-2}$]	υ_1	T [mm]
$1.3 \cdot 10^{-10}$	0.28	0.18	0.08	0.37	1

Numerical solution with finite element analysis

The numerical simulation of the interaction between the arm and sleeve was performed within the ABAQUS/CAE modelling environment with an explicit approach. Surface-to-surface contact was applied to simulate the interface interactions between the arm and sleeve. The impact condition was set to soft contact, which assumes that the two impact surfaces instantaneously acquire the same velocity in the direction of the impact. The soft contact relationship allowed penetration of the slave surface into the master surface at the constraint locations and allowed the transfer of tensile stress across the interface. When the surfaces were in contact, any contact pressure could be transmitted between them with no limits on magnitude. The friction coefficient between the arm and the sleeve was assumed to be 0.1. The interactive force was exerted on the compression sleeve or the arm against its normal direction of contact points. The penalty contact algorithm was employed to enforce contact constraints between the slave surface nodes (inner surface of sleeve) and the master surface (arm surface). In the whole putting process, bones were assumed to have few displacements in the x, y, and z directions of the global coordinates in the boundary.

Figures 3(a)-3(d) illustrate the simulated magnitudes and distribution of arm surface pressure during the dynamic wear process at four different moments, respectively. It can be seen from fig. 3 that as the sleeve moved from the styloid of the radius to the end of the upper arm, significant variation in the compression distribution and magnitudes occurred on the arm surface, which were closely related to the stretch states and mechanical functions of the sleeve fabrics. Figures 4(a)-4(d) depict the simulated stress distribution of the sleeve at the corresponding four time points during dynamic wear.

At the initial stage, figs. 3(a), 3(b), 4(a), and 4(b), the upper arm part of the sleeve was pulled over the styloid of the radius and forearm of the arm. Incompletely stretched sleeve fabric produced a lower interface pressure in the first stage, figs. 3(a) and 4(a). With the thickening of the arm and more areas of the sleeve gradually in contact with the arm surface, and sleeve fabric produced more stress and multidimensional mechanical deformations that included extension, shearing, bending and compression, which induced more interface

pressure on the arm. The pressure at the elbow was relatively high, figs. 3(c) and 4(c), which may be due to the larger circumference and protrusion of the elbow. At the end stage, figs. 3(d) and 4(d), the greatest stress was found in the areas around the end of the upper arm, followed by other parts of the upper arm and the elbow. The pressure on the arm and the stress of compression sleeve increased gradually as the circumference of the arm increased and changed with the changing of the physiological curve of the arm surface. The pressure values of the convex surfaces of the arm were relatively larger, while the pressure values of the concave surfaces were relatively smaller. Since human arms are complex irregular cylinders with different surface curvatures, the sleeve fabric does not achieve uniform contact everywhere, so uneven pressure is produced over different parts of the arm. Overall, pressure profiles of the arm are closely related to the change in sleeve stress; moreover, the changes in sleeve stress are more significant than those in the arm pressure profiles, which may be because sleeve fabrics are easily deformed.

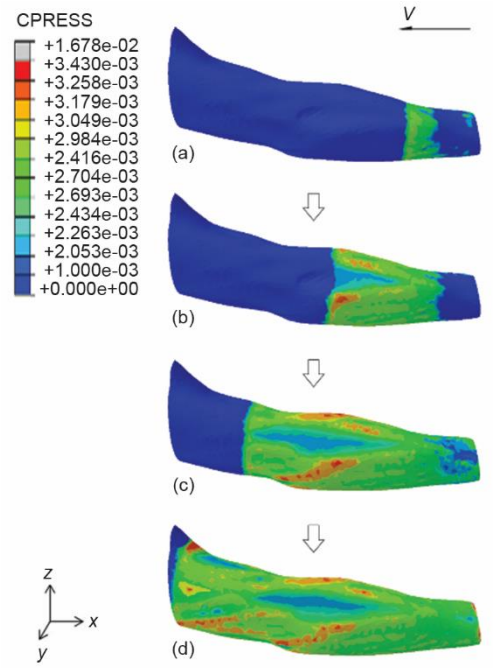

Figure 3. Simulation of pressure distribution on arm during dynamic wearing; (a) wearing the arm sleeve to one quarter, (b) wearing the arm sleeve to one half, (c) wearing the arm sleeve to three quarters, (d) wearing the arm sleeve completely

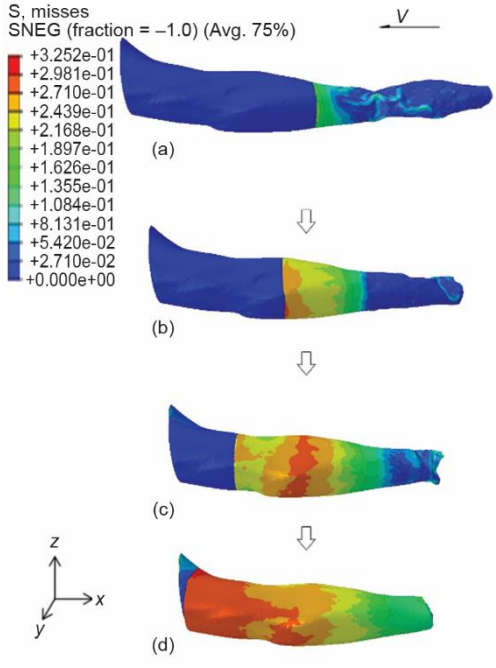

Figure 4. Simulation of stress distribution on sleeve during dynamic wearing; (a) wearing the arm sleeve to one quarter, (b) wearing the arm sleeve to one half, (c) wearing the arm sleeve to three quarters, (d) wearing the arm sleeve completely

Validation

To verify the pressures predicted by the simulation, the garment pressures that were exerted onto the human arm were measured and compared with those predicted by the FEM. To test the garment pressure systematically and comprehensively, the compression sleeve previously mentioned was put on the arm of the female subject for dividing grids before testing. As shown in fig. 5, the notation of every grid column is composed of numbers, while that

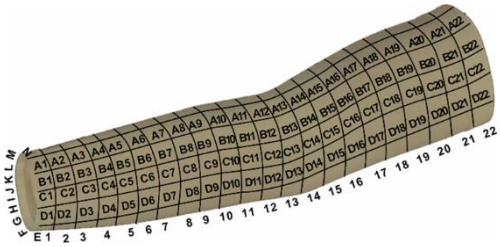

Figure 5. Compression sleeve with grid marks

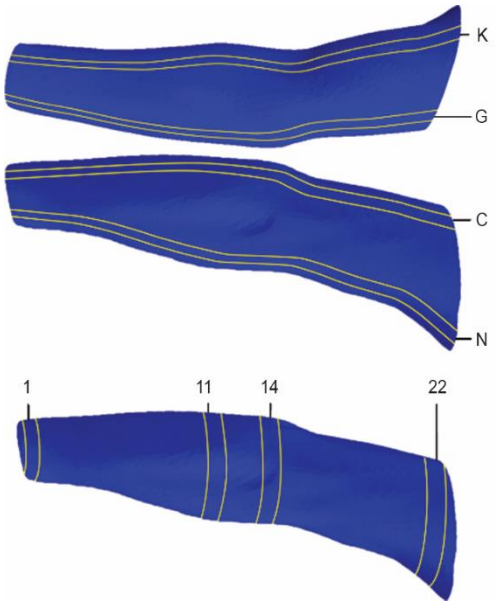

Figure 6. Several representative positions of the human arm

of every row is composed of letters, *i. e.*, the grids that run down from the top of the first left column are named A1, B1, C1, … , to N1, and the grids of the first row from the left to the right are named A1, A2, A3, … , to A22. In the simulation model, the simulated pressure applied to the elements on the arm surface of each grid was regarded as the average of the contact pressures given by the sleeve in the normal direction within the grid. The values obtained from the pressure measurement device were compared with prediction values by the FEM at the corresponding locations. To better compare simulated pressure with measured pressure values, four representative rows and columns on the human arm were selected, as shown in fig. 6. Positions 1, 11, 14, and 22 are the starting points of the arm wrist, the maximum circumference position of the forearm, the elbow joint of the arm and the upper arm end of the arm, respectively. The C, K, G, and N are the medial line of the arm, the lateral line of the arm, the outer edge line of the ulna at the lower end of the arm, and the outer edge line of the radius at the upper end of the arm, respectively.

The results of the pressure simulation and the sensor measurements at different locations over the arm given by the sleeve are shown in figs. 7 and 8, respectively. All of the simulated pressure values from the FEM and the sensor measured pressure values on representative rows and columns of the arm were between 2656 ~ 3323 Pa, which meet the requirement of suppressing growth and flattening hypertrophic scars caused by serious burns [3]. The simulated pressure values provided by the FEM show a similar changing trend with the measured values for every representative row and column on the arm. The simulation model developed by the FEM has good accuracy in predicting the sleeve-skin interface between the compression sleeve and the arm, the overall difference is no more than 7%, and there are only slight differences (only 0.1%) in some locations. Furthermore, fig. 8 also shows that the garment pressure increases gradually as the circumference of the arm cross-section increases along with changes in the physiological curve of the arm surface. In short, the simulated values have shown a good agreement with the experimental measured values within reasonable pressure ranges, which provides us a new engineering design approach for the prediction and improvement of compression garment products pressure functional performances.

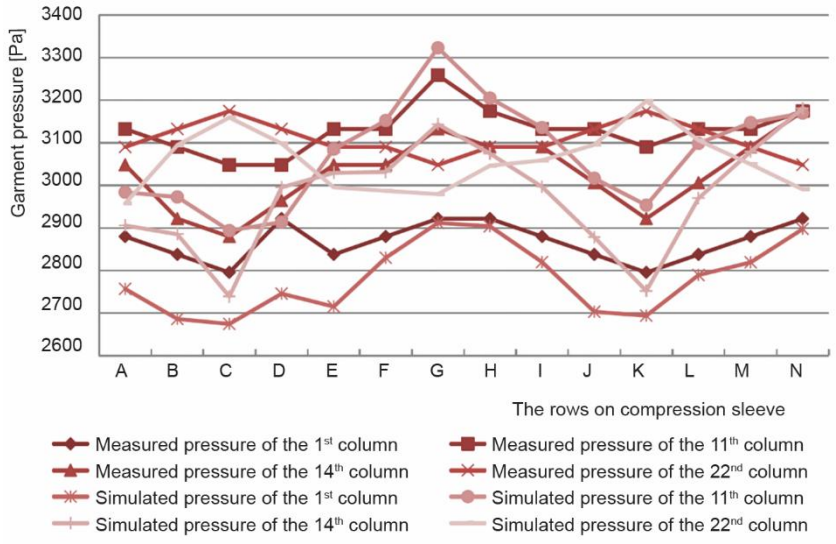

Figure 7. Comparison of simulated pressures from FEM and sensor measured pressures on representative columns (1, 11, 14, and 22) of arm induced by sleeve

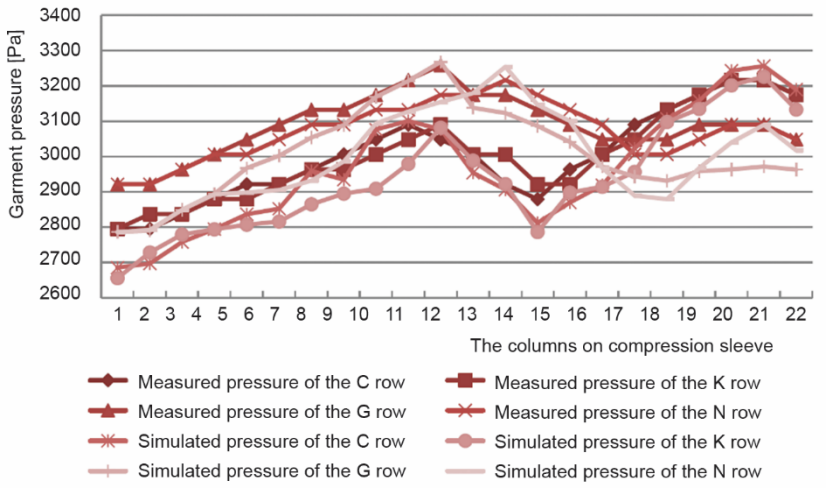

Figure 8. Comparison of simulated pressures from FEM and sensor measured pressures on representative rows (C, K, G, and N) of arm induced by sleeve

Conclusions

To optimize the design of compression garments through pressure objective testing and numerical simulation, a new 3-D biomechanical mathematical model is suggested for numerical approach to sleeve deformations, surface pressure magnitude, and distribution of arm and mechanical interactions between the human arm and sleeve during wear. The simulated model has consistently shown good agreement with experimental measurements within reasonable pressure ranges and can help to understand the overall contact pressure magnitudes and distribution over the arm.

There are some limitations in this study. The arm model used in the FEM was a normal hand without hypertrophic scars. Hypertrophic scars can develop with a wide range of different shapes, sizes, colors, and softness according to the condition of the wound of the injury, personal healing system, treatment received, *etc*. However, the parameters of the hypertrophic scars were not considered in the study, and properties of a real burned arm cannot be accurately reflected. To improve the practical use of the simulated model, it is important to have a model that considers the geometry of the hypertrophic scars and their mechanical properties. Nevertheless, the present study demonstrated the feasibility of the development of the pressure simulation model using the FEM. The simulation model developed can be used as a preliminary means for further development and improvement of garment pressure prediction.

If we want to study the effect of the porous structure of the garment on the pressure distribution, the two-scale thermodynamic model has to be adopted using fractal calculus [15-24], we will discuss the application in a forthcoming paper.

Acknowledgment

We would like to thank the China Scholarship Council for funding this research (No. 201809345023).

References

[1] Gauglitz, G. G., *et al.*, Hypertrophic Scarring and Keloids: Pathomechanisms and Current and Emerging Treatment Strategies, *Molecular Medicine*, *17* (2011), 1-2, pp. 113-125
[2] Li, P., *et al.*, The Recovery of Post-Burn Hypertrophic Scar in a Monitored Pressure Therapy Intervention Programme and the Timing of Intervention, *Burns*, *44* (2018), 6, pp. 1451-1467
[3] Bera, M., *et al.*, Influence of Linear Density of Elastic Inlay Yarn on Pressure Generation on Human Body, *Journal of Industrial Textiles*, *46* (2016), 4, pp. 1053-1066
[4] Makabe, H., *et al.*, A Study of Clothing Pressure Developed by the Girdle, *Journal of the Japan Research Association for Textile End-uses*, *32* (1991), 9, pp. 424-438
[5] Gaied, I., *et al.*, Experimental Assessment and Analytical 2D Predictions of the Stocking Pressures Induced on a Model Leg by Medical Compressive Stockings, *Journal of Biomechanics, 39* (2006), 16, pp. 3017-3025
[6] MacIntyre, L., New Calibration Method for I-scan Sensors to Enable the Precise Measurement of Pressures Delivered by 'Pressure Garments', *Burns*, *37* (2011), 7, pp. 1174-1181
[7] Rong, Liu., *et al.*, Effects of Material Properties and Fabric Structure Characteristics of Graduated Compression Stockings (GCS) on the Skin Pressure Distributions, *Fibers and Polymers, 6* (2005), 4, pp. 322-331
[8] Maklewska, E., *et al.*, Modelling and Designing of Knitted Products Used in Compressive Therapy, *Fibers & Textiles in Eastern Europe*, *14* (2006), 5, pp. 111-113
[9] Wong, A. S., *et al.*, Influence of Fabric Mechanical Property on Clothing Dynamic Pressure Distribution and Pressure Comfort on Tight-Fit Sportswear, *Sen'i Gakkaishi, 60* (2004), 10, pp. 293-299
[10] Luo, X. N., Luo, H. M., A Computing Model of Pressure Distribution from Tight Underwear, *Journal of Computational and Applied Mathematics, 195* (2006), 1-2, pp. 106-112
[11] Tarrier, J., *et al.*, Applying Finite Element Analysis to Compression Garment Development, *Procedia Engineering, 2* (2010), 2, pp. 3349-3354
[12] Dan, R., *et al.*, Numerical Simulation of the Relationship Between Pressure and Displacement for the Top Part of Men's Socks, *Textile Research Journal, 81* (2011), 2, pp. 128-136
[13] Yu, A., *et al.*, Numerical Simulation of Pressure Therapy Glove by using Finite Element Method, *Burns*, *42* (2016), 1, pp. 141-151
[14] Rohan, P. Y., *et al.*, Prediction of the Biomechanical Effects of Compression Therapy on Deep Veins Using Finite Element Modelling, *Annals of Biomedical Engineering, 43* (2015), 2, pp. 314-324
[15] Ain, Q. T., He, J. H. On Two-Scale Dimension and Its Applications, *Thermal Science, 23* (2019), 3B, pp. 1707-1712

[16] He, J. H., Ji, F. Y., Two-Scale Mathematics and Fractional Calculus for Thermodynamics, *Thermal Science, 23* (2019), 4, pp. 2131-2133
[17] He, J. H., *et al.*, A New Fractional Derivative and Its Application to Explanation of Polar Bear Hairs, *Journal of King Saud Universe Science*, *28* (2016), 2, pp. 190-192
[18] He, J. H., Li, Z. B., A Fractional Model for Dye Removal, *Journal of King Saud Universe Science*, *28* (2016), 1, pp. 14-16
[19] Liu, H. Y., *et al.*, Fractional Calculus for Nanoscale Flow and Heat Transfer, *International Journal of Numerical Methods for Heat & Fluid Flow*, *24* (2014), 6, pp. 1227-1250
[20] Liu, H. Y., *et al.*, A Fractional Nonlinear System for Release Oscillation of Silver Ions from Hollow Fibers, *Journal of Low Frequency Noise Vibration and Active Control*, *38* (2019), 1, pp. 88-92
[21] Wang, Q. L., *et al.*, Fractal Calculus and Its Application to Explanation of Biomechanism of Polar Bear Hairs, *Fractals, 26* (2018), 6, 1850086
[22] Wang, Q. L., *et al.* Fractal Calculus and Its Application to Explanation of Biomechanism of Polar Bear Hairs, (vol 26, 1850086, 2018), *Fractals*, *27* (2019), 5, ID 1992001
[23] He, J. H., A Simple Approach to One-Dimensional Convection-Diffusion Equation and Its Fractional Modification for E Reaction Arising in Rotating Disk Electrodes, *Journal of Electroanalytical Chemistry, 854* (2019), ID 113565
[24] He, J. H., Variational Principle for the Generalized KdV-Burgers Equation with Fractal Derivatives for Shallow Water Waves, *J. Appl. Comput. Mech., 6* (2020), 4, pp. 735-740

Paper submitted: May 5, 2019
Paper revised: November 1, 2019
Paper accepted: November 2, 2019